Peptide-mediated route to biomimetic collagen intrafibrillar mineralization

By Aya Kirahm Cloyd

Scholar Aya Kirahm Cloyd
B.S., University of Texas at Dallas, 2019

Submitted to the graduate degree program in Bioengineering Program and the Graduate Faculty of the University of Kansas in partial fulfillment of the requirements for the degree of Master of Science.

Chair: Dr. Candan Tamerler

Dr. Paulette Spencer

Dr. Malcolm Snead

Date Defended: 1 December 2022

The thesis committee for Scholar Aya Kirahm Cloyd certifies that
this is the approved version of the following thesis:

Peptide-mediated route to biomimetic collagen intrafibrillar mineralization

Chair: Dr. Candan Tamerler

Date Approved: 16 December 2022

Abstract

Overcoming short lifespan of current dental adhesives remain a significant clinical need. Adhesives rely on formation of hybrid layer to adhere to dentin, and penetrate within collagen fibrils. Achieving complete enclosure of demineralized collagen fibrils by monomers to fill in and close spaces is recognized as unattainable. We developed a peptide-based approach enabling collagen intrafibrillar mineralization and tested our hypothesis on a type-I collagen-based platform. Peptide design incorporated collagen binding and remineralization mediating properties using domain structure conservation approach. The structural changes from representative members of different peptide clusters were generated for each functional domain. Common signatures associated with secondary structure features and the related changes in the functional domain were investigated by the attenuated total reflectance Fourier-transform infrared (ATR-FTIR) and circular dichroism (CD) spectroscopy, respectively. Assembly and remineralization properties of the peptides on the collagen platforms were studied using atomic force microscopy (AFM). Mechanical properties of the collagen fibrils remineralized by the peptide assemblies was studied using PeakForce-Quantiative Nanomechanics (PF-QNM)-AFM. Engineered peptide was demonstrated to offer a promising route for collagen intrafibrillar remineralization. Proposed approach offers a platform to develop multifunctional strategies including different bioactive peptides, polymerizable peptide monomers and adhesive formulations as a step towards improving long-term prospects of composite resins.

Acknowledgments (optional)

I would to thank my committee members for their wisdom and guidance through this academic journey and my fellow lab mates for their technical, mental, and emotional support throughout this whole process.

Table of Contents

List of Figures

List of Tables

1 Introduction

The polymeric restorative materials have revolutionized the treatment of dental caries owning to *in situ* tissue engineering approaches introduced on the resin-dentin bonding (Ezazi et al.; Fischer et al.; Spencer, Ye, Kamathewatta, et al.; Ye et al.). Despite of the significant advances in composite resins treating tooth decays, the low durability of the current dental adhesives continues to be a major health burden. The Global Oral Health Status 2022 report released by the world health organization (WHO) estimated 2 billion people suffering from caries in their permanent teeth worldwide (Wen et al.). The retention of composite resins relies on the adhesive system, which infiltrates into the collagen matrix to adhere to dentin (Ezazi et al.; Song et al.; Hardan et al.; Spencer, Ye, Song, et al.; Iliev et al.). Adhesion and adhesive performance on dentin are especially challenging due to the complexity of dentin which is a mineralized dynamic biological tissue composed of 70% hydroxyapatite (HA), 30% type I collagen and non-collagenous proteins and water (Goldberg et al.; Marshall; Sarikaya, Ye, et al.). Due to the multifaceted events taking place at this complex resin-dentin adhesive interface, strategies developed so far have been slow to address the short-life span of resin-dentin bonding and subsequently prevent the repeated failure of composite resin restorations (Sarikaya, Song, et al.; Spencer, Ye, Kamathewatta, et al.).

The resin-dentin bonding can be accomplished through acid-etching to remove the mineral phase which provides space to facilitate the infiltration of the adhesive system into the collagen matrix of dentin. Structurally homogeneous infiltration of the resin monomers is difficult. Monomers are expected to fill the interfibrillar spaces within the collagen network and polymerized in situ to fully seal the region (Munchow and Bottino; Ye et al.; Spencer, Ye, Song, et al.; Oestervemb). However, the resulting resin-dentin interdiffusion zone suffers from poor

infiltration of resin monomers into the demineralized dentin matrix (collagen network). Penetration capacity of the monomers, pathology of the caries, expanded state of dentin collagen structure and the variation on mineral content affect the integrity of resin-dentin interdiffusion zone. Unbound and entrapped water in the collagen network further accelerates the hydrolysis of collagen and intensifies the vulnerability at this hybrid layer.

Despite the numerous approaches that have been developed to eliminate residual water from the collagen network, residual water is trapped within the hybrid layer. The residual water interferes with adhesive polymerization, plasticizes the adhesive and facilitates hydrolysis of the ester bonds in methacrylate-based adhesives. The carboxylate and alcohol by-products of the ester hydrolysis are even more hydrophilic than the original adhesive network, thus increasing water sorption into the hybrid layer causing a cascade of degradation (Frassetto et al.; Ye et al.; Zhang et al.; Song et al.; Spencer, Ye, Song, et al.; Iliev et al.; Amin et al.; de Brito, de Oliveira and Monteiro). This self-perpetuating cycle is aggravated by the insufficient infiltration of adhesive into the demineralized dentin collagen (Betancourt, Baldion and Castellanos; Reis et al.). Thus, leaving water-rich collagen fibrils exposed with a highly porous nature and allowing efficient sorption into the adhesive. Over time degradation reaches a point where microleakage starts to occur, with a diffusion of oral fluids (containing e.g. salivary esterase) and bacteria (e.g. *S. mutans*) (Balhaddad; Munchow and Bottino; Ye et al.; Zhang et al.; Reis et al.; de Brito, de Oliveira and Monteiro; Muliyar et al.). This accelerates the degradation cascade of the adhesive, thus compromising its bond integrity, furthering tooth demineralization and caries progression at the site – resulting in the ultimate failure of the restoration (Frassetto et al.; Ye et al.; Zhang et al.; de Brito, de Oliveira and Monteiro; Oestervemb). The unprotected collagen fibers have a

highly porous structure. Strategies that enable achieving better penetration and protecting the collagen network would be key to interfacial stability at the complex dentin-adhesive interface.

Biomineralization is a complex process that involves cellular participation and the proteins regulating mineral deposits and structures. During the mineral growth, living systems adapted progressive dehydration. Dentin collagen mineralization contains non-collagenous proteins and self-assembled collagen fibrils acting as stabilizers while guiding the mineral growth. Collagen mineralization is considered to be mediated by interactions between negatively charged complexes of amorphous calcium phosphate (ACP) precursors with the collagen fibers. The ACPs precursors are formed due to interactions between ionic components with the proteins controlling the mineral deposition and phase transformation precipitation. The ACP precursors penetrate into the collagen fibrillar matrix and then transform in hydroxyapatite resulting in the excellent mechanical properties observed in mineralized tissues including dentin. Developing better understanding of the biomineralization processes and mechanisms accelerated the biomimetic design strategies for tissue repairs. Non-collagenous proteins composed of mainly acidic residues and their analogs were proposed to direct the mineralization at these soft-hard tissue interfaces (Moradian-Oldak and George). Statherin, a short salivary protein or statherin derived peptide sequences or acidic amino acids or peptides that involves acidic amino acids due their abundance in non-collagenous proteins were proposed to attract calcium and phosphate ions to stabilize and prevent degradation at the dentin-adhesive interface (Wang et al.; Tian et al.; Steinbauer et al.). Some of these bioinspired approaches are very promising as early concept studies. These studies also provide the increasing interest to study bio-hybrid approaches at the collagen interfibrillar platforms that mimics the hybrid layer at the dentin-adhesive interdiffusion zone.

Inspired by nature, our group has been focusing on biomimetic approaches in designing complex materials and interfaces. Processes and mechanisms underlying biomineralization is particularly intriguing and involves progressive dehydration. Using combinatorial and computational approaches, our group has been designing peptides with specific affinity for inorganics including calcium-phosphate minerals (Ca-P). Prior work with these peptides showed that these molecules induced calcium phosphate mineralization by exhibiting control over the mineralization kinetics and mineral morphology under specific conditions. We reported phage display selected hydroxyapatite binding peptide (HABP: MLPHHGA) and reported mineralization properties in constraint and unconstraint forms (Gungormus et al.). These peptides can be used to generate novel biological agents where they can be combined with another bioactive peptide or protein. We also demonstrated that the resulting multifunctional properties of these agents can be further improved using computational modeling and predictive tools. By designing HABP and fluorescent proteins, we demonstrated can be used in labelling mineralized tissues and remineralization of deficient dentin surfaces. These peptides can be further conjugated with a monomer and keep their bioactive property as they conform into polymeric network. Our recent studies include a “bio-hybrid” adhesive, that is designed to include HABP or an antimicrobial peptide conjugated with a methacrylate monomer and demonstrated to preserve the peptide activities in the resulting the polymeric network (Frassetto et al.).

Intrafibrillar remineralization of collagen at the “hybrid layer” could be the key to address the vulnerability of the exposed demineralized dentin collagen and improve long-term repair of the tooth (Niu et al.). Recent approaches for the intrafibrillar remineralization with peptides involve using the casein phosphopeptide-amorphous calcium phosphate complex (Zhou et al.;

Sattabanasuk et al.), beta-sheet self-assembled peptide hydrogels (P11-4 (de Sousa et al.), ID8 (Li et al.), RAD/KLT (Xia et al.)), amelogenin peptide P26 (Mukherjee et al.), and mineralization-promoting peptides (MMP3 (Gungormus, Ozdogan, et al.; Gungormus and Tulumbaci)) among others. These methods either focus on mineral formation at the site or involve stabilizing the collagen fibrils by generating a scaffold to achieve intrafibrillar mineralization (Bermudez et al.). While all these approaches could be promising, none of these approaches are specifically targeting collagen while the mineral deposition is taking place in the collagen interfibrillar sites. A platform that enables to study different approaches while targeting collagen could contribute to the design of a hybrid layer with improved properties.

In this study, we propose an approach that builds upon an engineered-peptide design by combining a collagen binding peptide with the hydroxyapatite binding peptide, connected by a spacer which minimizes interdomain interactions in order to physically direct collagen self-assembly and remineralization to achieve intrafibrillar mineralization at the site. This study advances a simple, dynamic, and flexible collagen self-assembly platform upon to test the activity and efficacy of the designed peptides. By combining linear HABP peptide, MLPHHGA, (Gungormus, Fong, et al.)) with a collagen binding peptide motif (TKKLTLRT), derived from de Souza *et al.* (1992) (Desouza and Brentani). By interrogating the spacer design approach combining experiment and computational approaches, we rationally designed the engineered multi-functional peptide and tested self-assembly and remineralization properties on the collagen platform. This peptide enabled collagen remineralization approach offers a platform to study several additional components including different peptides, peptide monomers and resin formulation to mimic the hybrid layer.

2 Materials & Methods

2.1 Materials

Peptide synthesis required N-methyl morpholine (NMM), Wang amide resin, Fmoc-resin, Fmoc-amino acid building blocks, D-biotin, piperidine, and 2-(1H-benzotriazole-1-yl)-1,1,3,3-tetramethyluranium hexafluorophosphate (HBTU) which were purchased from AAPPTec LLC (Louisville, KY, USA). N, N-Dimethylformamide (DMF, 99.8%), trifluoroacetic acid (TFA, 99%), triisopropylsilane (98%), thioanisole (99%), and diethyl ether (99%) were obtained from Sigma-Aldrich (St. Louis, MO, USA). 1,2-ethanedithiol (95%), N,N Diisopropylethylamine (99.5%, nitrogen flushed), and hydroxymethyl (Tris) aminomethane hydrochloride (Tris-HCl, 99%+, extra pure) were purchased from Acros Organics (NJ, USA). Phenol (89%), calcium chloride dihydrate (99.7%) and sodium hydroxide (97%) were obtained from Fisher Scientific (Fair Lawn, NJ, USA). Glycerophosphate calcium salt was purchased from MP Biomedicals LLC (Solon, OH, USA) and 6N Hydrochloric acid solution from Fisher Chemical (Fair Lawn, NJ, USA). All chemicals in this study were used without further purification. We acquired FastAP Thermosensitive Alkaline Phosphatase from Thermo Fisher Scientific (Vilnius, Lithuania). Collagen Type 1 solution from rat tail (3mg/mL, C3867, 95%) was purchased from Sigma-Aldrich (St. Louis, MO, USA). Highest grade V1 12mm Mica discs and 12mm atomic force microscopy specimen discs were obtained from Ted Pella Inc. (Redding, CA, USA). STKYDOT, an atomic force microscopy specimen disc adhesive, was purchased from Bruker Corporation (Camarillo, CA, USA).

2.2 Peptide Design

The selection of the collagenase-collagen binding peptide (CBP) sequence, TKKLTLRT, was based as an analog of the original peptide sequence, TKKTLRT, reported by de Souza *et al.*

(1992) (Desouza and Brentani). The latter corresponds to the amino acid sequence derived from the nucleotide sequence of the complementary DNA strand coding for the human pro-α2(I) collagen domain, attacked by human fibroblast collagenase. de Souza *et al.* used the principle of hydropathic complementarity to develop a peptide sequence that would result in sense collagen domain-to-antisense peptide sequence binding given respective hydrophobic-hydrophilic residue interactions (Blalock and Smith; Brentani "Biological Implications of Complementary Hydropathy of Amino-Acids"; Brentani "Complementary Hydropathy and the Evolution of Interacting Polypeptides"). Employing that same principle, analogs to TKKTLRT were explored to identify hydropathic profiles that show better alignment with respect to the amino acid sequence of the sense strand of the gene. From this, the sequence TKKLTLRT was chosen to be implemented. In addressing the biomineralization prong of this study, the hydroxyapatite binding peptide (HABP1) sequence (MLPHHGA) was selected. The sequence was developed by Gungormus et al. (2008) (Gungormus, Fong, et al.) where it showed the highest binding affinity in directing the mineralization process of calcium phosphate (Ca-P). This study examines a novel bifunctional peptide, CBP-HABP1, by combining these two motifs, separated by a short and rigid spacer: TKKLTLRT-APA-MLPHHGA.

2.3 Peptide Synthesis

The CBP, HABP1, and CBP-HABP1 peptides were synthesized on the AAPPTEC Focus XC synthesizer (AAPPTec, Lousiville, KY, USA), using a standard Fmoc solid-phase peptide synthesis protocol. The peptides were synthesized on Wang resin with the subsequent resin-bound peptides cleaved and their sidechains deprotected, resulting in the canonical C-terminus functional group of carboxylic acid. The cleavage cocktail of CBP contains the following: TFA, phenol, triisopropylsilane, water (90 : 5 : 2.5 : 2.5). For HABP1, the cleavage cocktail is as

follows: TFA, thioanisole, ethanedithiol, triisopropylsilane, water (87.5 : 5.0 : 2.5 : 2.5 : 2.5). Lastly, the cleavage cocktail for the bifunctional peptide CBP-HABP1 contains: TFA, phenol, thioanisole, water, ethanedithiol, triisopropylsilane (81.5 : 5.0 : 5.0 : 5.0 : 2.5 : 1.0). The peptides were let in cleavage cocktail, on a rotator, for 2 hours, precipitated in cold ether, and then lyophilized.

Crude peptide purification was performed on a semi-preparative reverse-phase high pressure liquid chromatography (HPLC) Waters system, containing Waters 600 controller and Waters 2487 Dual Absorbance Detector, using a 10μm C-18 silica Luna column (250x10mm, Phenomenex Inc., CA, USA). The mobile phase is composed of phase A (94.5% HPLC grade water, 5% acetonitrile, 0.1% TFA) and phase B (100% acetonitrile). Lyophilized peptides are dissolved in 4mL of phase A and purified at 0.5% phase B*min^{-1} on a linear gradient (5%-85% phase B), performed at 3mL*min^{-1}, room temperature, with detection at 254nm. Purified fractions collected were verified by analytical Shimadzur HPLC system, comprised of LC-2010 HT liquid chromatograph and SPD-M20A prominence diode array detector, with a 5μm C-18 silica Luna column (250x4.6mm, Phenomenex Inc., CA, USA). This mobile phase is composed of phase A (99.9% HPLC-grade water, 0.1% TFA) and phase B (100% acetonitrile) with the system run on a linear gradient with 1mL*min^{-1} flow, 40°C, detection at 254nm. The purified peptides (CBP, HABP1, CBP-HABP1), were then lyophilized and stored at -20°C.

2.4 Fourier Transform-Infrared Spectroscopy (FT-IR)

The molecular structures of our peptides were verified using the PerkinElmer Frontier IR spectrometer with the universal attenuated total reflectance polarization accessory (Waltham, MA, USA). Lyophilized peptide was evaluated across the wavelength range of 4000 cm^{-1} – 550 cm^{-1} at a 4 cm^{-1} spectral resolution.

2.5 Circular Dichroism (CD)

The secondary structure of each of the three peptides, CBP, HABP1 and CBP-HABP1 were measured through circular dichroism (CD) spectra. Measurements were made with CD spectrometer (JASCO, J-815) at room temperature, using a 1.0 mm cuvette. Each peptide sample was dissolved at 0.2 mg/mL in 10 mM potassium phosphate (pH 7.4) at 4 °C for 16 h. Spectra shown are averaged from three experimental repeats. The scans were acquired from 190 to 300 nm at a scanning speed of 60 nm/min. CD spectra were processed for secondary structure composition with the tools of CD Pro. For each peptide, the reference set selected was SMP50. The fractions of secondary structure (Regular Helix, Distorted Helix, Regular Sheet, Distorted Sheet, Turns and Unordered) were averaged for all three CD Pro tools (SELCON3, CDSSTR, and CONTILL).

2.6 Collagen-peptide sample preparation

Grade V1 round mica, 0.21mm thick and 12mm diameter, was used as the substrate surface and mounted onto a 12mm atomic force microscopy specimen disc using STKYDOT adhesive. In 1 mL of 3mg/mL Type 1 rat tail collagen suspension, 50 nanomoles of peptide. The ratio of mass collagen to mass peptide ranges from 100 wt collagen: 1 wt peptide for single domains to 100 wt collagen: 3 wt peptide for the chimeric peptide. Once peptide is dissolved and gently mixed in the collagen suspension, 150μL is drop-cast onto the substrate surface and left to self-assemble at 4°C for 16 hours. The preparation resulted in mica surfaces with a coating completely dried by visual inspection.

2.7 ALP-driven mineralization of collagen-peptide functionalized substrate

ALP-driven mineralization was executed following the protocol discussed in Gungormus et al. (2008) (Gungormus, Fong, et al.). The mineralization buffer prepared was composed of 24.4

Ca^{2+} mM, 14.4mM B-glycerophosphate made in 25mM Tris-HCl buffer at pH 7.4, and 200μL/well is added to a 24-well plate. Collagen-peptide samples were placed gently within the well to lay flat at the bottom. The mineralization reaction was initiated by adding FastAP (thermosensitive alkaline phosphatase), 1.4 x 10^{-6} g/mL, and left to incubate at 37°C for 20 minutes. The samples were then removed from the wells, gently rinsed in sterile-filtered water, and left to air dry overnight. Throughout this process the samples were handled in a horizontally flat manner to prevent disturbing the peptide-functionalized collagen layer on the surface of the substrate.

2.8 RAMAN spectroscopy

Demineralized dentin samples, adhesive/dentin samples (pre/post mineralization), and SC collagen on glass were imaged using LabRAM ARAMIS Raman microscope (HORIBA Jobin Yvon, NJ, USA), equipped with a HeNe laser (λ= 663 nm, laser power = 17 mW). Light micrograph images were taken using a 50X long working distance objective Olympus lens. The samples spectra were evaluated over a wavelength range of 300 cm^{-1} – 1800 cm-1 with a 15s spectra acquisition time at 4 acquisitions per cycle, and processed using LabSPEC 6 software (HORIBA Jobin Yvon, NJ, USA).

2.9 Peak Force-QNM AFM imaging

Bruker Multimode 8 HR scanning probe microscope (Bruker Nano Inc., Camarillo, CA, USA) was operated in tapping mode using PeakForce Quantitative Nanomechanics (PeakForce-QNM) in air mode conditions (24 ± 2 ◦C, 40% ± 5% RH) in order to examine the topographical and elastic property changes of the collagen-peptide samples both before and after mineralization. Tapping mode etched silicon probes, type RTESPA 525-30 (Bruker Nano Inc., Camarillo, CA, USA) with a resonant frequency of about 518 kHz, were used to acquire images (1μm x 3μm and

5μm x 5μm) at scan rate of 0.5 Hz with 512 pixel/line resolution. The images of the samples were recorded using NanoScope 8.15 software and analyzed using NanoScope Analysis 2.0 software.

2.10 SEM/EDS imaging of mineralized collagen-peptide samples

In order to examine initial intrafibrillar mineral formation, morphology and determine Ca/P ratios precipitated on the peptide-functionalized collagen surface, a Cold Field Emission Scanning Confocal Microscope (SEM, S-4700 model, Hitachi High-Tech America, Schaumburg, IL, USA) equipped with a silicon drift energy-dispersive detector (EDS, X-max, Oxford Instruments, Concord, MA, USA) was used via the Microscopy and Analytical Imaging Research Resource Core Laboratory (RRID:SCR_021801). Collagen-peptide samples were sputter-coated with 3nm gold using a Quorum sputter coating system (Q150, Quorum, Laughton, East Sussex, UK). SEM imaging was completed at an acceleration voltage of 10kV at ultra-high resolution operating mode and EDS measurements were made at 10kV under normal operating mode to preserve the integrity of the collagen-peptide layer and prevent burning during signal capture. EDS analysis was done through Aztec software (Oxford Instruments, Concord, MA, UDA).

2.11 SEM surface mineral mapping

SEM images were analyzed to examine the Ca-P mineral deposition changes between the different peptide-functionalized collagen platforms and to understand the relative amount of initial Ca-P mineral formed on those surfaces. The SEM images were processed through written code using Python 3.9.13 software (Appendix C). The *tif* files were preprocessed by median blurring and histogram equalization. Multi-Otsu threshold determination algorithm was applied, resulting in a binary matrix, with 1 corresponding to the location of mineral surface and 0

corresponding to a location of no mineral surface. The area of that represents the surface mineral. The resulting binary image represents the surface mineral area, and the percent-area is the proportion of mineral surface locations to all locations in the image.

3 Results

To begin our exploration, we began comparing RAMAN microscopy signatures of human dentin to that of the rat tail Type 1 collagen, which is used to build out platform for testing our peptide activity and efficacy. Two-dimensional RAMAN light microscopy examined the differences in chemical signature between demineralized dentin and intact dentin on a tooth specimen. Figure 1A shows the light micrograph representation of the two regions, with Figure 1B reflecting the respective spectral analysis. In intact dentin, the peaks consistent with $CaPO_4$ and CO_3^{2-} are observed at 960 cm^{-1} and 1070 cm^{-1} respectively. The intensity of these mineral bands decreased in the demineralized dentin, whereas the spectral signatures reflecting collagen became clearer: 1667cm^{-1} (amide I), 1460 cm^{-1} (amide II), the doublet observed from 1215 cm^{-1} to 1310 cm^{-1} (amide III) (Lin, Li and Cheng; Oladepo et al.; Spencer, Ye, Kamathewatta, et al.). The chemical signatures observed in both intact and demineralized dentin were then compared to rat tail type 1 collagen spin-coated (SC) on glass, with and without undergoing ALP-driven mineralization, using RAMAN as well. The indicative collagen peaks observed in demineralized dentin and the mineral peaks seen with intact dentin were respectively observed in the SC collagen and the mineralized SC collagen on glass. As well, in mineralizing the SC collagen, the amide peaks observed prior were diminished as a result.

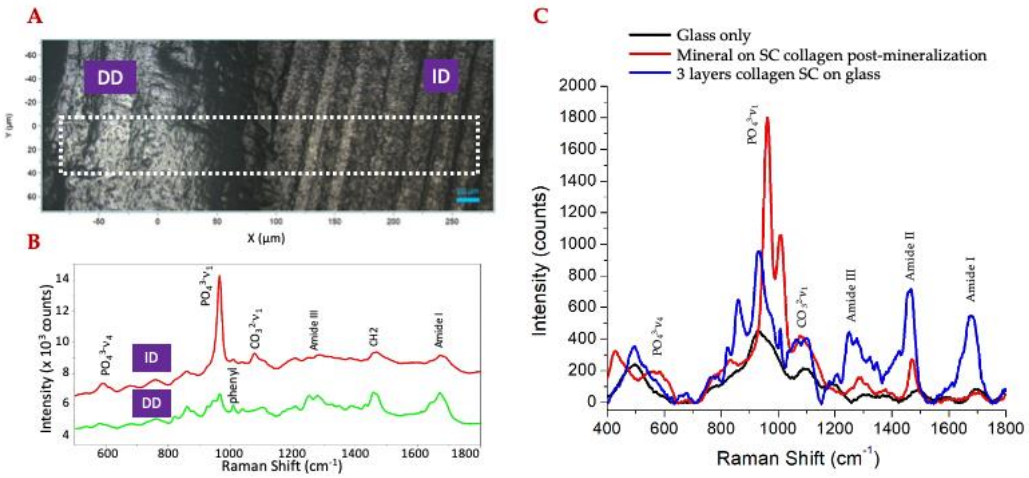

Figure 1. Human dentin profile **A)** RAMAN light microscopy image at 50X over 400μm x 140μm area, marked regions comparing demineralized dentin (DD) to intact dentin (ID)(Spencer, Ye, Kamathewatta, et al.); **B)** RAMAN spectra of DD and ID highlighted regions(Spencer, Ye, Kamathewatta, et al.). **C)** RAMAN spectra of rat tail SC on glass pre/post 60 minutes of ALP-driven mineralization.

Now establishing the similarity human dentin components and the rat tail type 1 collagen being used as our platform, we then moved to evaluating the use of HABP1 (MLPHHGA) to potentially direct mineralization within the adhesive/demineralized dentin hybrid layer. To do this we used Divisive Clustering Analysis (DCA), a hierarchical k-means clustering method which is useful for identifying the internal structure of multi-layer datasets. Figure 2A shows 2D Raman spectroscopy with and without HABP1 incorporation into the adhesive/dentin specimen, following mineralization procedure. Figure 2A shows that HABP1 forms mineral with a RAMAN peak consistent with $CaPO_4$ formation (960 cm^{-1}) which does not appear after the mineralization procedure without peptide. Figure 2B further analyzes the 2D Raman spectra, with coloring being applied by the DCA method. The DCA method measures similarity in three dimensions: ratio of 960/1460 peak (any mineral to collagen with retained amide II structure), ratio of 1078/960 (gradient mineral carbonation: carbonate to any mineral) peak, ratio of the 960/1667 peaks (any mineral to collagen with retain amide I structure). 1460 cm^{-1} is the amide II peak for collagen, and 1667 cm^{-1} is the amide I peak for the collagen used. The 960 cm^{-1} peak is the phosphate peak present in any calcium phosphate mineral; 1078 cm^{-1} is a peak for carbonate.

The method clusters the following groups: collagen only, mineral group I and mineral group II. This analysis method is hierarchical, meaning that the mineral groups discovered are the mineral formation groups which are most distinctive. The distinction between the mineral groups is from how much collagen is present at the location of the mineral, how much the present collagen's two noted amide peaks signature are maintained and by how much carbonate is in the mineral.

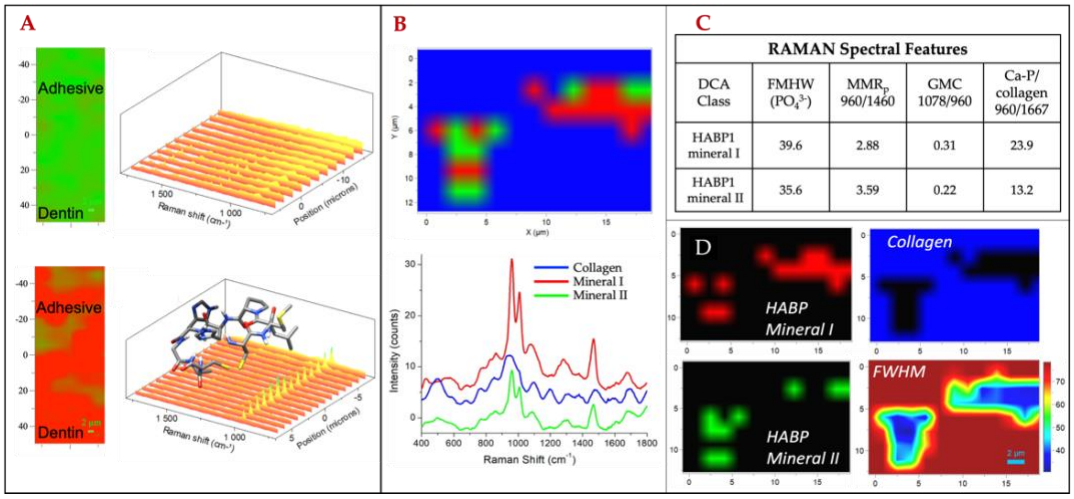

Figure 2. Spectral analysis of HABP-functionalized surfaces **A)** RAMAN DCA with spectral analysis adjacent of A/D interface pre/post ALP-driven mineralization with HABP1 present. **B)** RAMAN DCA of mineralized surface with HABP1 on mineral types present and corresponding spectral analysis. **C)** RAMAN spectral features evaluated over both HABP1 mineral types observed. **D)** Isolated DCA mapping of collagen, HABP1 Mineral group I, HABP1 Mineral group II, and full width at half maximum (FWHM) spatial mapping.

Figure 2C shows that Mineral group I has higher peaks for mineral (960 cm^{-1}), has less retained amide II structure for the collagen, more carbonate absorbance per mineral absorbance and more retained amide I structure of the collagen. 1667 cm^{-1} has previously been noted as a beta-sheet structure(KONG and YU). Mineral group II has more amide II peak retained (1460 cm^{-1}). Since the sample is evenly coated with collagen, this means that where the Mineral group II formed, induced structure of the collagen by the mineral has more amide II peak retained but less amide I peak (1667 cm^{-1}) retained. This mineral has less carbonate compared to Mineral group I. Because of the lower carbonate content, we propose that Mineral group II is a more mature mineral formation closer to hydroxyapatite and Mineral group I. Figure 2D shows where

the two mineral groups are in the two panels on the left. The top right panel shows where the Raman sees only mainly collagen, and the bottom left panel is the signal for where the mineral is, where blue denotes more mineral absorbance and red denotes less mineral absorbance. Comparing the bottom left FWHM spectra to the two mineral groups on the left, we see that the mineral groups are not explainable exclusively by how much mineral absorbance occurs at a location. This shows that we are able to distinguish the activity of HABP1 with respect to the background collagen and produce mature biomimetic mineral. Thus, demonstrating its potential, when co-assembled with collagen, to direct biomimetic intrafibrillar mineralization at this complex interface.

To extend the remineralization capability beyond the dentin-adhesive interface, we designed a chimeric peptide sequence combining collagen binding and remineralization domains. Using PEP-FOLD3, we compared folded structures of the chimeric peptide sequence with the corresponding folded domains alone. Our motivation is that structural change in the incorporated chimeric peptide domain relates to change in the function of the domain. This balance is explored through the comparisons of spacers with varying flexibility and length (Figure 3).

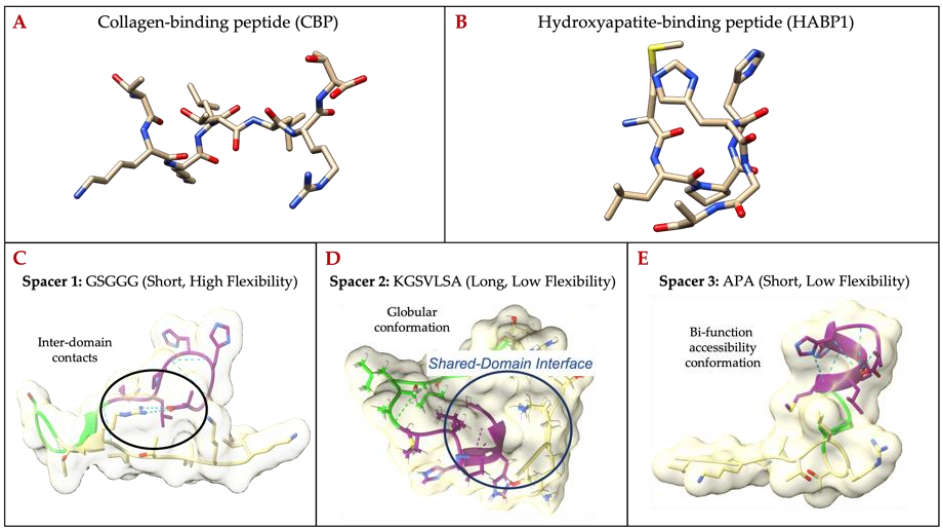

Figure 3. Effect of spacer on folded peptide structure. Folded peptide structures generated by PEP-FOLD3 **A)** CBP and **B)** HABP1. Building chimeric peptide CBP-HABP1: **C)** short spacer with high flexibility, ex: GSGGG; **D)** long spacer with low flexibility, ex: KGSVLSA; **E)** short spacer with low flexibility, APA.

The spacers fit into three general categories according to the inter-domain relationships: 1) inter-residue contacts 2) globular conformation and 3) bi-function accessibility conformation. The inter-residue contacts limit the conformational flexibility of the domains the most directly, while the globular conformation limits the accessibility of the domain surfaces through shared interfaces by the domains. We investigated helical motifs with low GRAVY scores (KGSVLSA, PKSALQEL) and high GRAVY scores (GLALLGWG, LGWLSAV, WLMNYFWPL and YLMNYLLPY). The limitation of these helical motifs was to form structures where the active domains shared interfaces. The most promising conformation type for retaining independent functions is the bi-functional accessibility conformation because the each domain has the most access to interact with its molecular recognition partner. APA was the spacer which had the greatest accessibility for the domains. We chose the APA spacer with low flexibility and a length which reduces the probability of inter-domain interactions. The spacer length and its backbone shape are keys to which inter-domain residue interactions, if any, are likely to induce conformational shifts between the domain structures. The functional domains of the chimeric peptide (Figure 4I-L) folded structure surfaces are orthogonal to each other in the structure views

shown in Figure 4. The domains do not form a hairpin-like structure in which the collagen-binding domain and the hydroxyapatite binding domain have contact residues with each other. Each of the single peptide domains (CBP Figure 4A-D, HABP1 Figure 4E-H) and the chimeric peptide (I-L) are shown with their electronegativity surface features. The provided structures are energy-minimized folded structures chosen as a cluster representative by PEP-FOLD3 (Lamiable et al.) and rendered by UCSF Chimera (Meng et al.).

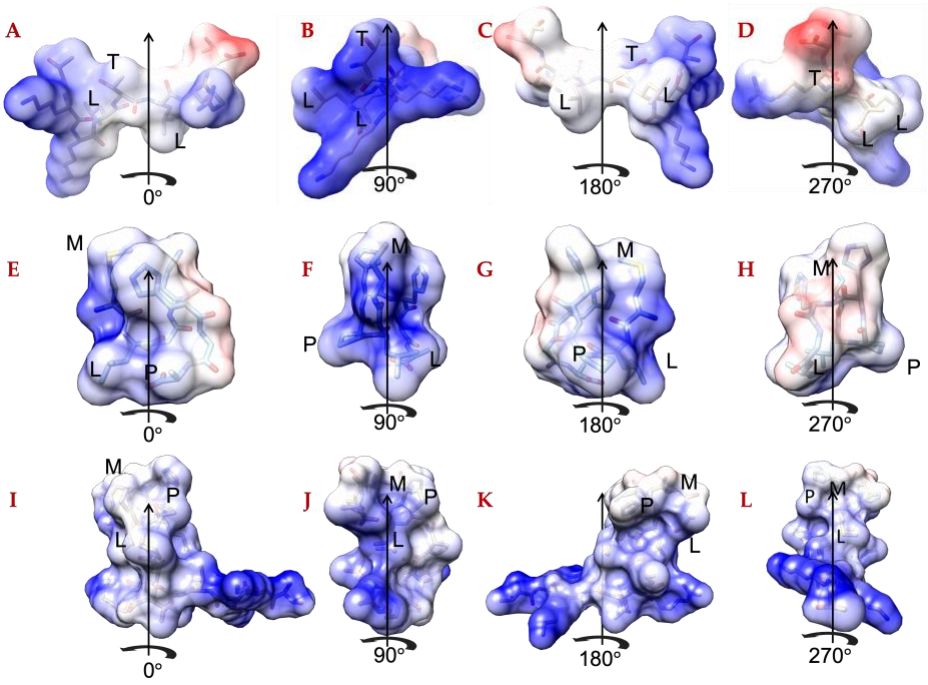

Figure 4. Electronegativity surface rotations of chimeric peptide (**A-D**) High-Stability Collagen Binding Peptide (TKK**LTL**RT), (E-H) HABP1 (**MLP**HHGA) and (**I-L**) Chimeric ColBP-APA-HABP1 (TKKLTLRT-APA-**MLP**HHGA). Underlined residues are labeled to orient the reader. The folded peptide structures were generated by PEP-FOLD3(Lamiable et al.).

Through this domain structure conservation approach analyzing each of the chimeric peptides with structures generated with PEP-FOLD3, we selected CBP-APA-HABP1 for synthesis. The secondary structures of the CBP, HABP1, and CBP-HABP1 were investigated in the lyophilized state in their respective FT-IR spectra (Figure 5). The Amide I band relates to the stretching of the backbone carbonyl. CBP-HABP1 and CBP have their highest Amide I band peak related to beta-sheet structures with peak absorbance at 1624 ± 1 cm^{-1} (KONG and YU).

CBP-HABP1 and CBP also share an Amide I peak of 1662 cm^{-1}, which is related to α-helix formation. The dominate peak for lyophilized linear HABP1 is at 1646 cm^{-1}, which is in the Random assignment region (KONG and YU). We observed a main peak at 3280 cm^{-1} in the Group A region (NH stretching) for both the CBP and HABP1 peptides, which was observed to be shifted to 3270 cm^{-1} with CBP-HABP1. All peptides contained the same maximum in the Amide II region (CN stretching and NH bending) at 1532 cm^{-1} and lacked peaks in the Amide III region (CN stretching and NH bending) (Figure 5).

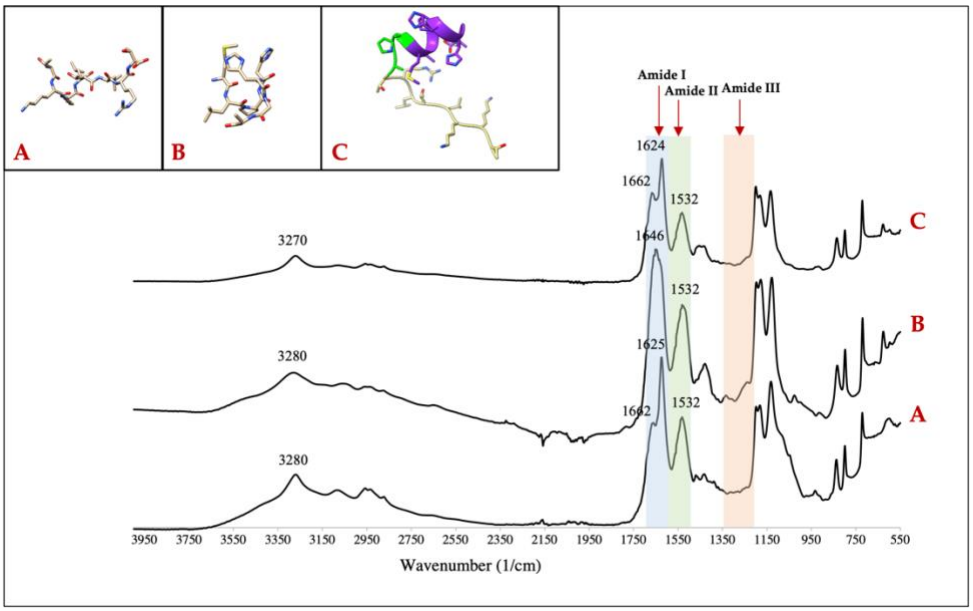

Figure 5. FTIR spectra of peptides **A)** Collagenase collagen binding peptide (CBP), sequence: TKKLTLRT. **B)** Hydroxyapatite binding peptide (HABP1), sequence: MLPHHGA. **C)** Bifunctional peptide (CBP-HABP1), sequence: TKKLTLRT-APA-MLPHHGA. All peptide ribbon images shown are side views. All synthesized peptides presented with corresponding FT-IR spectroscopy confirming molecular structure.

Next, we investigated the *in vitro* structural changes for dissolved peptides. Figure 6 shows the changing secondary structure properties of the peptides estimated through CDPro (Sreerama and Woody). Figure 3D shows the change in secondary structure composition of the chimeric peptide compared to the mean secondary structure compositions of the single functional domains. Since the composition change for all the features were 10% or less, we decided to

evaluate the functionality to determine if changes of this size in secondary structure features makes any measurable impacts on the chimeric domain functions.

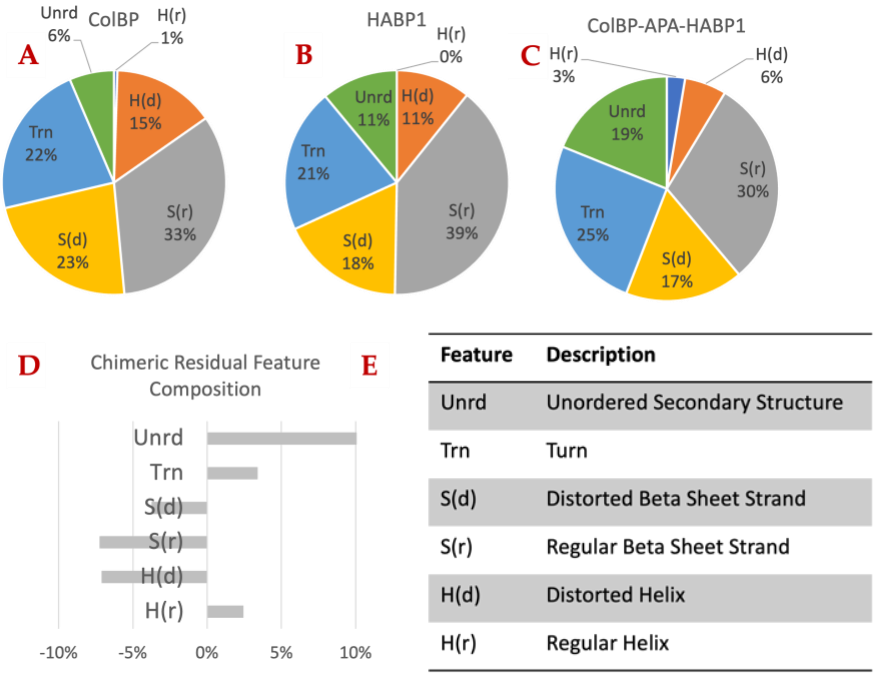

Figure 6. Circular dichroism additivity analysis of peptides. Circular dichroism additivity analysis comparing the average structure feature composition of among functional domains (A,B) to the chimeric peptide (C) which contains both functional domains and a 3-amino acid spacer. The residuals given in (D) are the difference between the feature composition from CD analysis and the average feature composition of the two domains. (E) Legend of feature descriptions in A-D. The chimeric peptide has about 10% more unordered structure than expected from the average of the functional domains. This loss of ordered structure seems to come mainly from the loss of regular beta sheet strand (S(r)) and distorted helix (H(d)).

3.1 Effect of peptide-functionalization on collagen self-assembly

From understanding the conformational flexibility of the peptide, it's important to examine the effect the respective peptide incorporation had on the self-assembly of the collagen fibrils on mica substrate (Figure 7). This was done using AFM topography image analysis to observe changes in the collagen fibril assembly. The images were acquired in tapping mode and presented as 5x5□m images with the color scale shown next to the image and the gradient change corresponding to observed surface features. Non-fibril features, indicated as intensity saturated regions on the surface, are acetic acid salt crystals leftover from the evaporation of the

solution in which the rat tail collagen was suspended. They were excluded from image analysis in order to prevent signal shadowing of the surface fibril assembly. Topographical analysis of the surfaces showed changes in the collagen fibril assembly with the incorporation of peptide in collagen prior to drop-casting (Figure 3). Collagen alone (Figure 3A) was observed to have an average fibril width of 98.890 nm, collagen-(CBP) showed a larger average fibril width of 121.442 nm, and collagen-(CBP-HABP1) exhibited an average 82.368 nm (Table 1). However, with collagen-(HABP1) the average fibril width rose to 129.877 nm, but the standard deviation more than tripled compared to that of the other samples (Table 1). We see in Figure 7C a mixture of larger fibrils as compared to fibrils formed with collagen alone (Figure 7A), or compared to fibrils formed with collagen-(CBP) (Figure 7B), or collagen-(CBP-HABP1) (Figure 7C).

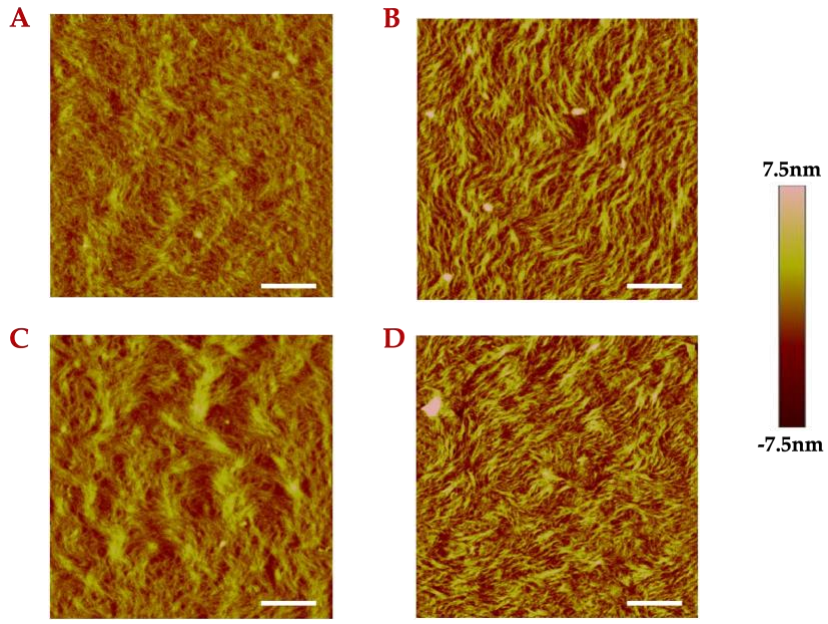

Figure 7. Effect of peptides on collagen fibrils. Collagen self-assembly examined through surface topography mapped via Tapping Mode AFM. Scale bar = 1μm. **A)** Drop-casted collagen. **B)** Drop-casted collagen with CBP. **C)** Drop-casted collagen with HABP1. **D)** Drop-casted collagen with CBP-HABP1.

Unpaired, two-tailed t-tests were performed ($p<0.05$) comparing the observed fibril widths between collagen functionalized with CBP-HABP1 (Figure 7D) and the controls (Figure 7A-C). Collagen-(CBP-HABP1) fibrils were measured to be smaller than collagen-alone fibrils,

resulting in a statistically significant difference. Though the average fibril width for CBP-HABP1 was observed less than that of the controls, it has a larger distribution of fibril sizes relative to the mean compared to collagen alone and collagen-(CBP) (Table 1), as observed in Figure 7D. Therefore, we see a distinct difference in the fibril width properties when CBP and CBP-HABP1 are incubated with collagen fibrils, implying binding interactions between collagen and these peptides.

Next, we consider the specificity of the interactions with collagen and their CBP, HABP1 or CBP-HABP1. We note that the fibril width standard deviation for the collagen-(CBP) is similar to the standard deviation of collagen-(CBP-HABP1). This finding implies specificity of binding between the collagen and CBP-HABP1 that missing between collagen and HABP1. The fibril width variation shows that the hydroxyapatite binding motif binds less specifically to collagen than either the collagen binding peptide or the chimeric peptide. Some of the non-specific interactions of HABP1 may be due to the increase in overall hydrophobicity than the collagen binding motif (Appendix A). HABP1's nonspecific interaction with collagen can influence the hydrophobic/hydrophilic dynamics in collagen fibril self-assembly(Hafner et al.). However, the non-specific binding character of HABP1 is not seen with the chimeric peptide, though the HABP1 sequence is within CBP-HABP1. The non-specificity of the HABP1 domain is mitigated by the presence of the collagen-binding domain in the chimeric peptide. This result implies that the free energy of binding between chimeric CBP and collagen is much lower than the free energy of binding between chimeric HABP1 and collagen. While the mitigation results in lower fibril width standard deviation for the chimeric peptide than the HABP1 domain alone, it still results in a higher standard deviation than with CBP alone. The collagen fibril width variation with chimeric peptide is much less than the average variation of the individual domains,

implying that collagen is much more likely to interact with chimeric CBP than with chimeric HABP1. The fibril assembly with CBP-HABP1 is seen in Figure 7C shows the wider variation of collagen fibril widths compared to collagen alone or to collagen-(CBP). When the chimeric CBP does interact with the collagen fibrils, its specific interactions differ from CBP because the mean fibril width reduces by about 30% compared to the single domain and a reduction of about 15% compared to collagen alone. Future studies can determine if the specific interactions are between the same collagen-contact residues for CBP and chimeric CBP, but conformational shifts reduce probability of those residues or if the contact residues change to include residues from the other functional domain.

Table 1. Statistics on fibril widths evaluated from AFM topographical imaging

	Collagen	**Collagen-(CBP)**	**Collagen-(HABP1)**	**Collagen-(CBP-HABP1)**
Mean (nm)	98.890	121.442	129.877	82.368
Standard Deviation	19.258	20.658	87.643	26.470
% of mean	19.47	17.01	67.48	32.14

3.2 Mechanical properties of peptide-functionalized collagen platform pre/post mineralization

Building on the observed effects of the chimeric peptide on the self-assembly of collagen, we then moved to examine the effects this change in assembly had on the mechanical properties of the collagen. Quantitative modulus mapping was executed via PeakForce-QNM AFM to observe the changes in the elastic modulus distribution of the surface given the chimeric peptide incorporation into the assembly. The elastic modulus is previously established to be derived by using the Derjaguin-Muller-Toropov (DMT) model and thus reported as the DMT modulus(Derjaguin, Muller and Toporov). Figure 8A shows the topographical view of the surface given each peptides incorporation as compared to the control, which all coincide with the effects observed and discussed in Figure 7. For the modulus mapping of those surfaces, Figure

8B, collagen alone shows a uniform, average lower elastic modulus, Figure 8C, across its surface as compared to when peptide affects its self-assembly. Collagen-(HABP1) shows a slightly higher modulus, Figure 8C, than the collagen control. It also shows little more variation given its modulus mapping, Figure 8B, due to its nonspecific influence on collagen fibril formation. Comparatively, CBP and CBP-HABP1 combined with collagen respectively show a higher average elastic modulus, Figure 8C. Given the specific interaction of collagen-(CBP) in forming thicker fibrils of collagen, as seen in Figure 8B, the corresponding increase in modulus, compared to collagen alone, is observed. This effect of function is maintained with CBP-HABP1 where we see its incorporation with collagen having the largest significant increase in modulus compared to collagen alone and when incorporated with peptides of the individual motifs. As seen with HABP1, CBP-HABP1 also shows a larger surface modulus variance, Figure 8B (Appendix B), compared to that of collagen alone and when combined with CBP. These results show a combinatorial nanomechanical effect dependent on how the peptide domains influence collagen fibril assembly.

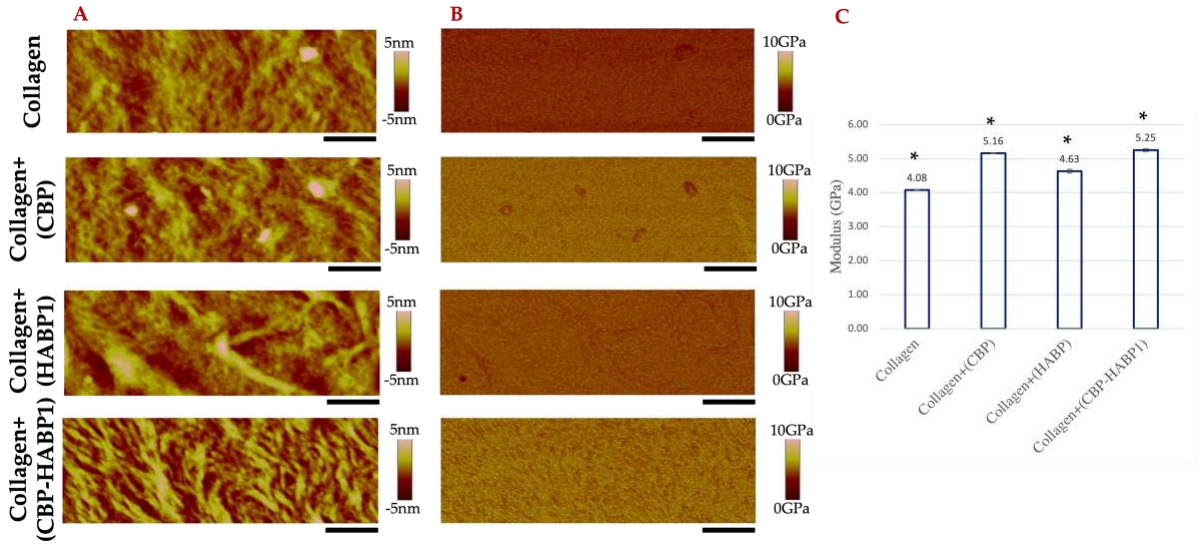

Figure 8. Mechanical properties of collagen control and peptide-functionalized collagen samples examined through PeakForce-QNM AFM. **A)** AFM 2D-Topographical view; **B)** DMT Modulus mapping; **C)** Modulus average per pre-mineralization sample, error bars indicating standard deviation, and significant difference ($p < 0.05$) represented as *. Scale bar = 500nm.

Following mechanical characterization of collagen-peptide formulations, the next step was to characterize and study the effects of biomimetic mineralization on those surfaces. ALP-driven mineralization was used to study the mineral formation on these surfaces given the contribution of ALP to the remineralization of dentin. The AFM analysis showed major topographical and morphological changes due to mineralization. The surfaces of the samples were rougher post-mineralization, Figure 9A, which may have resulted from collagen fibril re-assembly corresponding with the Ca-P mineral formation, both surface and sub-surface. The topographical mineral characteristics mapped seem to change between the collagen control and the peptide-functionalized collagen samples, as seen in Figure 9A. These differences between mineral formations are subsequently reflected in the modulus mapping, Figure 9B. Each step of peptide incorporation, comparing the motifs individually to the chimeric, show different elastic modulus characteristics of the mineral formed on the respective surfaces. The average moduli examined in Figure 9C show statistically significant changes between pre- and post-mineralization moduli per surface. Collagen alone showed the largest increase in elastic modulus, followed by collagen-(HABP1) which also exhibited the largest standard deviation. The larger moduli of collagen and collagen-(HABP1) can be attributed to the potential supersaturation of mineral in the collagen substrate layer on the mica. For the collagen control, this is due to unsupervised mineral formation. Whereas with HABP1, given its random nonspecific interaction with collagen it is plausible that non-uniform distribution of HABP1 in the collagen substrate layer would result in more variations in peptide concentration at the surface. This would lead to greater variation of mineral formation at the substrate surface, as supported by the larger variance observed with HABP1 compared to the rest of samples, collagen control included (Figure 9, Table S2). On the other hand, collagen-(CBP) and collagen-(CBP-HABP1) both show the smallest significant

increase in elastic modulus post-mineralization, with collagen-(CBP-HABP1) having the lowest elastic modulus post-mineralization compared to the rest. We observe that smaller variations in mechanical properties implies more consistent locating of peptide within the collagen substrate. While combining the peptide domains retains the consistent collagen substrate locating for both CBP and CBP-APA-HABP1, we have yet to determine how the mineralization kinetics and morphology result in the observed mechanical properties. This limited change in elastic modulus pre- and post-mineralization of collagen-(CBP-HABP1) and resulting lower post-mineralization modulus may be due to an unknown effect of the chimeric peptide's conformation, once bound to collagen, on the activity of the hydroxyapatite binding motif.

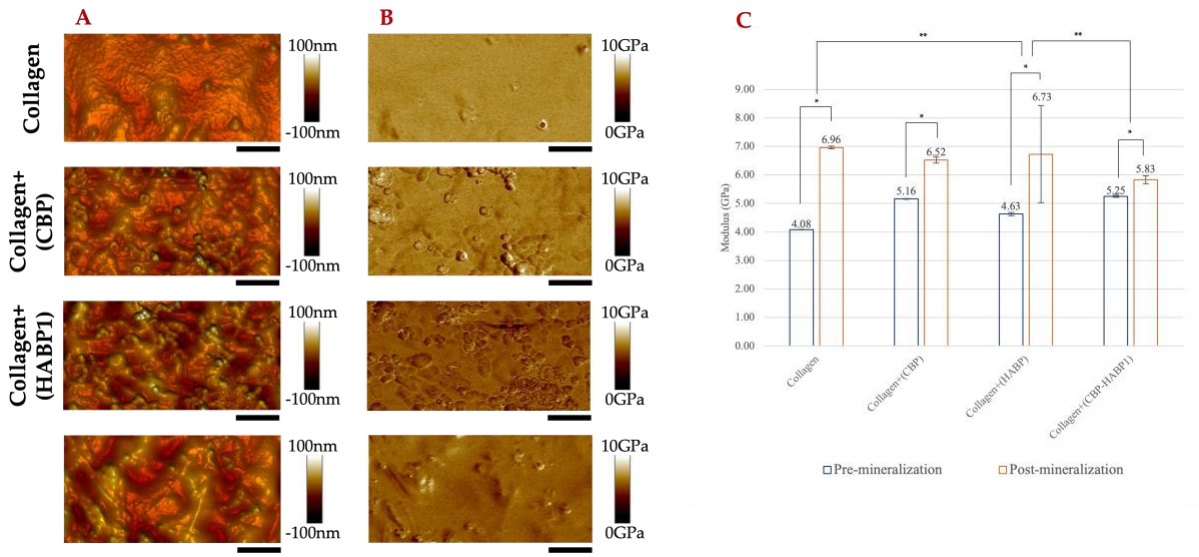

Figure 9. Characterization of peptide-functionalized collagen surfaces after 20 minutes of ALP-driven mineralization examined through PeakForce-QNM AFM. **A)** AFM 3D-Topographical view, **B)** Modulus mapping through the DMT modulus, and **C)** comparison between pre- and post-mineralization per sample represented as averages over the area, error bars representing standard deviation, and significant difference ($p < 0.05$) represented as *. Scale bar = 1μm.

3.3 Examining the Ca-P deposits on the peptide-functionalized collagen platform

Building on the examinations of resulting mechanical properties shifts due to ALP-driven mineralization on the peptide-functionalized collagen platforms, we then moved to analyze the composition and morphology of the Ca-P deposits on those surfaces through SEM/EDS, as seen

in Figure 10. The EDS results validated the finding of Ca-P mineral isomorphs on the peptide-functionalized collagen platforms, from which we calculated the calcium/phosphate ratios to examine compositional differences. Mineralized tissues contain a wide span of Ca-P ratios, ranging between 1.33 to 1.67. The initial mineral formed in the collagen alone and collagen-(HABP1) platforms had an average Ca-P ratio of 1.40 and 1.41 respectively. Collagen+(CBP) and collagen+(CBP-HABP1) had comparatively lower average Ca-P ratios, at 1.30 and 1.25 respectively. The molar ratio of the former two fall between that of octacalcium phosphate and amorphous calcium phosphate (ACP), each 1.33 and 1.50 respectively(Woolfolk et al.; LeGeros; Sheikh et al.; Meyer et al.).

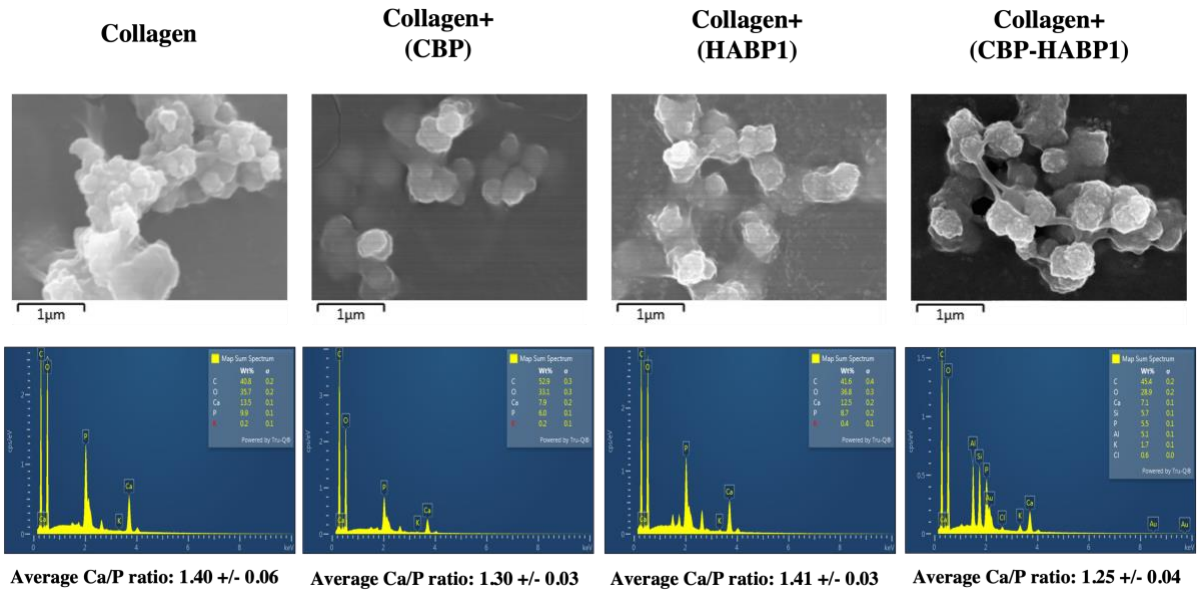

Figure 10. Mineral deposition on peptide-functionalized collagen via SEM images with corresponding EDS spectra. Ca/P averages displayed below EDS spectra, calculated across minimum three unique areas per peptide-functionalized collagen sample. **A)** Drop-casted collagen; **B)** Drop-casted collagen+(CBP); **C)** Drop-casted collagen+(HABP1); **D)** Drop-casted collagen+(CBP-HABP1). Scale bar is under each image, 1mm.

As observed, with or without the incorporation of HABP1, the mineral morphology remains the same. However, with the incorporation of TKKLTLRT (collagen-binding motif), the Ca-P ratio significantly decreases. This shift could be due to TKKLTLRT (collagen-binding motif) potentially affecting the activity of HABP1, due to change in conformation, causing there to be

higher monobasic Ca-P formation during mineralization resulting in lower average Ca-P ratios. The effect on activity is coupled with what's similarly observed in Figure 9A-C**,** showing a lower modulus on the collagen platforms where TKKLTLRT is incorporated. This combined with the shift to lower Ca-P ratio is overall conserved from collagen-(CBP) to collagen-(CBP-HABP1).

After understanding the mineral morphology on the peptide-functionalized collagen platforms, the spatial mapping of the mineral formed on those surfaces were examined, Figure 11. The surfaces are shown at 30,000X and processed using Multi-Otsu thresholding algorithm, separating surface and subsurface mineral formation along with any background noise. Comparing mineral formations on original SEM images, collagen and collagen+(CBP) both show branched columnar mineral growth, whereas collagen+(HABP1) and collagen+(CBP-HABP1) show more extensively branched columnar mineral growth as well as plate-like mineral growth.

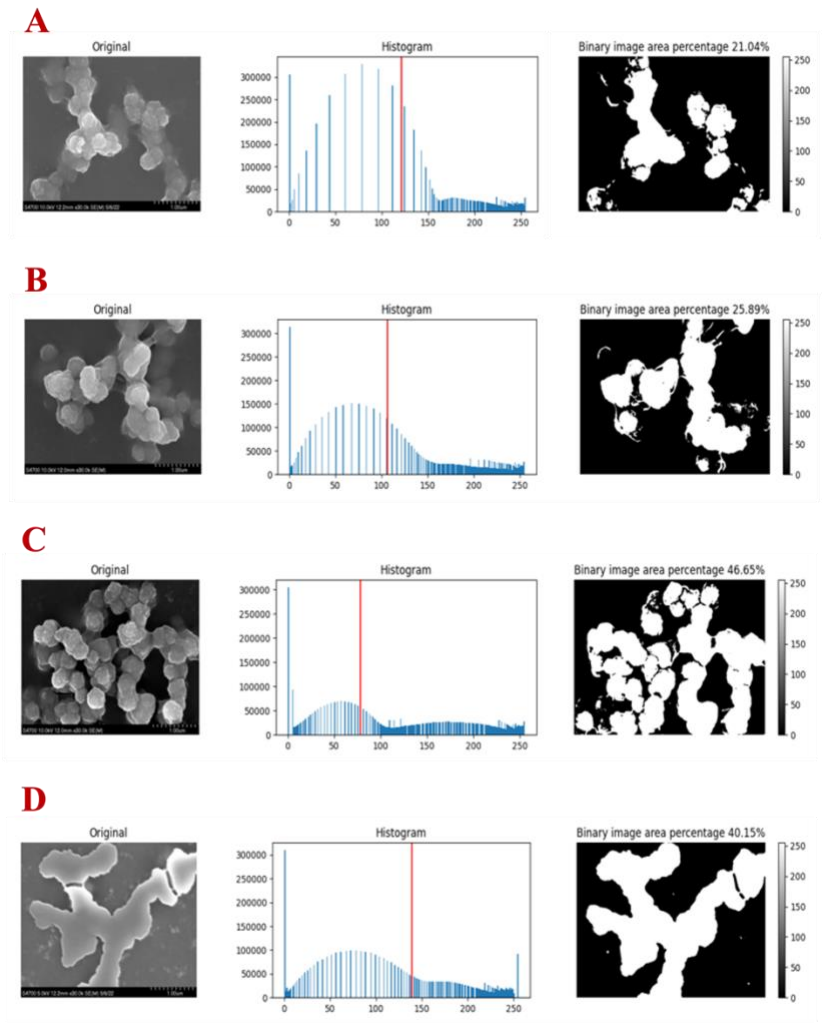

Figure 11. Mineral deposition mapping on SEM of peptide-functionalized collagen samples. Magnification level 30,000X. The first image, in the 3x1 array per condition, is the original SEM image, the second is the histogram of frequency of pixels per bin (0 to 255) within the SEM image, and the third is the binary conversion of the histogram based on the multi-Otsu threshold indicated by the red line on the histogram. Gradient scale indicated on the right. **A)** Drop-casted collagen; **B)** Drop-casted collagen+(CBP); **C)** Drop-casted collagen+(HABP1); **D)** Drop-casted collagen+(CBP-HABP1).

In evaluating the area covered by the mineral over the surface from the Multi-Otsu calculations, the collagen+(CBP-HABP1) showed similar mineral area covered to collagen+(HABP1), double of that observed with collagen and collagen+(CBP). Collagen+(CBP-HABP1)'s histogram distribution was also similar to that of collagen+(HABP1), indicating a similar mineral growth amount at their respective locations, compared to the others at the surface. This supports the preservation of HABP1 activity in the chimeric peptide. Thus,

showing more robust mineral formation reflecting an increase in mineral kinetics with the inclusion of the motif in the chimeric peptide, when co-assembled with the collagen.

4 Discussion

This study is further investigation of our research into the development of a self-strengthening peptide-functionalized dental adhesive that improves the integrity and durability of the adhesive/dentin (a/d) interface. Our previous work focused on improving the adhesive through the development of peptide-tethered-polymer systems (Yuca et al.) and self-strengthening adhesive formulations(Ezazi et al.; Sarikaya, Song, et al.). The engineered peptide (CBP-HABP1) and collagen self-assembly platform investigated in the current study concentrated on affected dentin within the a/d interface.

Within the collagen self-assembly platform, CBP-HABP1 exhibited conserved activity for its collagen binding motif. AFM topography data showed thicker and organized fibril assembly with the incorporation of the peptide in the platform— such topography was not observed with HABP1. The results with CBP-HABP1 and CBP can be attributed to the fact that both peptides contain the collagen-binding motif, thus likely binding to the collagen, in part, through sense-antisense domain interactions (Desouza and Brentani). Whereas with HABP1, its non-specific interactions with the collagen fibrils attribute to the larger range of fibril widths observed with its incorporation. As an *in vivo* comparison, collagen fibrils formed in dentin have a diameter range of 80-100nm that self-assemble in a hierarchical manner between 2nd tier (microfibrillar) and 3rd tier (fibrillar) levels(Bertassoni and Swain; Habelitz et al.). The platform we worked with allowed such hierarchical progressions of fibrillogenesis to be observed. On top of which CBP-HABP1 showed average fibril diameter within the range observed for dentin, without the need for assistance for proteoglycans. Meaning CBP-HABP1 alone would be able to direct collagen fibril self-assembly in deficient dentin without relying on native noncollagenous proteins(Goldberg et al.).

The intramolecular interactions of collagen self-assembly as mediated by CBP-HABP1 showed overall improvement in the nanomechanical properties of the collagen platform. CBP-HABP1 may not only align with the collagen but also bring mineral formation to the point of binding to the fiber, via the hydroxyapatite binding motif, thus mimicking tissue interfaces in intrafibrillar mineralization(Hafner et al.). Given this, the reason as to why a lower elastic modulus was observed with CBP-HABP1 post-mineralization is currently unknown. This could be since the peptide is intrinsically disordered, this gives it greater flexibility in its secondary structure conformations thus affecting the relative activity of the motifs. This platform provides a model of how the theoretical function through conformation is characterized in the real output of said function. Through spacer modification, this could be further investigated on this platform in order to optimize the function of both the collagen binding and hydroxyapatite binding motifs in the chimeric peptide, naturally extending beyond to probing other motif combinations (e.g. antimicrobial (Yuca et al.)). This further extends the potential dynamic and versatile nature of the collagen self-assembly platform.

Early-stage mineral formation, prior to stages reaching octacalcium phosphate (molar Ca-P ratio, 1.33) has so far been minimally investigated. Here with CBP-HABP1 integrated in the collagen self-assembly platform is observed lower molar Ca-P ratios than octacalcium phosphate, while still observing plate-like and cylindrical morphologies reported with mineral in dentin(Habelitz et al.). It is possible that a form of amorphous calcium phosphate is being observed since its seen in transient phases when forming Ca-P minerals in aqueous environments, showing as low as 1.18 Ca-P molar ratios in early transient forms(Meyer et al.; Dorozhkin and Epple). As Ca-P mineral chemical composition is strongly dependent on pH and surrounding calcium phosphate ion concentrations, further studies with this platform examining

longer mineralization times while monitoring buffer pH changes as well as mineralization done under different pH conditions is vital. Given the *in vivo* microenvironmental pressures created by the resident *S.mutans* in demineralized dentin at the adhesive/dentin interface, it is crucial to investigate and further optimize the intended peptides ensuring optimal function(Scharnow, Solinski and Wuest; Jayaraj and Ganesan; Vahedi et al.; Hegde et al.; Iijima et al.; Buzalaf et al.).

Our findings not only confirm the bifunctional activity of CBP-HABP1 but also demonstrate micro and nano level detection is possible with the collagen self-assembly platform for the respective motif functions present within the chimeric peptide. This demonstrates the flexible and dynamic potential of this platform for investigating activity and efficacy of different engineered peptides, initial mineral formation, and intrafibrillar mineralization. This is one step in the direction of a peptide-polymer hybrid dental adhesive system to remineralize caries-affected dentin, prevent adhesive hydrolytic degradation, and subsequently increase the lifespan of dental restoration.

5 Conclusion

Dental caries is the most ubiquitous infectious disease of mankind resulting in destruction of the teeth and recognized as a global health crisis (Woolfolk et al.). Composite resins are widely adapted in restorative dentistry, but their short lifespan leads to a cycle of repeated replacement and an inherent risk of pulpal injury, loss of tooth structure and weakened tooth. The leading cause of composite restoration failure is recurrent decay. In contrast to dental amalgam, composite lacks the capability to seal gaps at the interface between the restorative material and tooth structure. The low-viscosity adhesive that bonds the composite to the tooth is intended to seal this interface, but the adhesive seal to dentin is fragile — it is readily degraded by oral fluids, enzymes, and acids. which would undoubtedly benefit from the longer durability of adhesive restorations to solve clinical problems related to restoration integrity and recurrent decays. The adhesive-dentin bond is a heterogeneous construct — its composition includes the hybrid layer, which ideally integrates adhesive with highly porous collagen fibers. Failure of the adhesive-dentin bond is the critical issue preventing long lasting dental restorations (Spencer, Ye, Song, et al.; Tsujimoto et al.; Ye et al.). The weaker link resulting in recurrent decays is the hybrid layer, which integrates highly porous collagen fibers. Following acid-etching, demineralized collagen fibrils contain contains trapped water, which is extremely difficult to remove. Achieving complete enclosure of demineralized collagen fibrils by monomers to fill in and close spaces is recognized as unattainable under clinical conditions. In nature, biomineralization adapted a progressive dehydration process where calcium phosphate precursors and proteins play a critical role in mineralizing the collagen interfibrillar domain, which results in excellent mechanical properties. We developed a bioinspired peptide-based approach enabling collagen intrafibrillar mineralization.

Chimeric peptide design incorporated collagen binding and remineralization mediating properties. We used a domain structure conservation approach in designing chimeric peptides with different spacer sequences and tested their structure-function relations. The selected chimeric peptide was tested on a type-I collagen-based platform. Peptides were studied for their self-assembly and remineralization properties on the collagen platforms. Engineered peptide was demonstrated to offer a promising route for collagen intrafibrillar remineralization. The proposed approach offers a platform to develop multifunctional strategies including different bioactive peptides, polymerizable peptide monomers and adhesive formulations as a step towards improving long-term prospects of composite restorations resins.

6 Appendix A: Biochemical properties of peptides

Peptide name & chemical properties	Peptide Sequence
CBP MW: 960.19 g/mol Theoretical pI: 11.17 Gravy Index: -0.850	TKKLTLRT
HABP1 MW: 761.90 g/mol Theoretical pI: 6.69 Gravy Index: -0.129	MLPHHGA
CBP-(linker)-HABP1 (CBP-HABP1) MW: 1943.34 Theoretical pI: 11.17 Gravy Index: -0.32	TKKLTLRT-(APA)-MLPHHGA

*Calculated using ExPasy ProtParam tool

7 Appendix B: Statistics on PeakForce-QNM DMT Modulus pre/post mineralization

	Pre-mineralization			
	Collagen	**Collagen-(CBP)**	**Collagen-(HABP1)**	**Collagen-(CBP-HABP1)**
Mean (GPa)	4.08	5.16	4.62	5.25
Standard Deviation (GPa)	0.010	0.018	0.057	0.039
Variance (GPa^2)	0.065	0.215	2.16	1.01
	Post-mineralization			
	Collagen	**Collagen-(CBP)**	**Collagen-(HABP1)**	**Collagen-(CBP-HABP1)**
Mean (GPa)	6.96	6.52	6.73	5.89
Standard Deviation (GPa)	0.483	0.107	1.708	0.140
Variance (GPa^2)	2.34	11.4	2.92×10^3	19.6

8 Appendix C: SEM image processing source code (Python 3.9)

```python
import numpy as np
from glob import glob
from pathlib import Path
from PIL import Image
import os
import cv2
from tqdm import tqdm
from matplotlib import pyplot as plt
from skimage.filters import threshold_multiotsu



# Path to the data directory
main_dir = Path("/INSERT PATH HERE")

# Set all tif files in within the data dir..
tifs = []
for child in os.listdir(main_dir):
    print(child)
    tifs.append(list((main_dir / child).glob("*.tif")))


def area_precentage(image):
    '''Calculate the area of the pixels above a certain threshold is fixed to zero'''
    pixels = len(np.column_stack(np.where(image > 0)))
    image_area = image.shape[0] * image.shape[1]
    area_ratio = round((pixels / image_area) * 100,2)
    return area_ratio

def findArea (image, name):
    #apply blur to remove the small bright spots
    image = cv2.medianBlue(image, 7)

    #equalize histogram
    eq_image = cv2.equalizeHist(image.ravel()).reshape((image.shape[0],image.shape[1]))

    # Find the thresholds in the histogram
    # Set any value less than the smallest threshold to zero results in a binary image
    (threshold, regions) = cv2.threshold(image, 0, 1, cv2.THRESH_BINARY | cv2.THRESH_OTSU)[1].astype(np.bool)

    #calculate the area of the binary image
    area = area_precentage(regions)

    # Visualize results
    fig, ax = plt.subplots(nrows=1, ncols=3, figsize=(15, 3))
    im_ratio = regions.shape[0]/regions.shape[1]

    # Plotting the original image
    im1  = ax[0].imshow(image, cmap='gray')
    ax[0].set_title('Original')
    ax[0].axis('off')

    # Plotting the histogram and the corresponding thresholds
    im2 = ax[1].hist(eq_image.ravel(), bins=255)
    ax[1].set_title('Histogram')
    ax[1].axvline(threshold, color='r')

    # Plotting the binary image
    im3 = ax[2].imshow(regions, cmap='gray')
    ax[2].set_title('Binary image area {:.3f}'.format(area))
    ax[2].axis('off')

    fig.colorbar(im3, ax=ax[2], orientation="vertical", fraction=0.047*im_ratio)

    plt.tight_layout()
    plt.show()
    fig.savefig('INSERT PATH HERE' + name + '_{}.png'.format(area))
    return np.uint8(regions)

# Iterate through loaded images
for i in tqdm(tifs):
    for file in i:
        name = str(file).split('\\')[-1].split('.')[0]
        image = np.array(Image.open(file))[:1790,:] # PIL is the easiest library to load tif into python
        regions = findArea(image, name)

```

9 Works Cited

"Global Oral Health Status Report Towards Universal Health Coverage for Oral Health by 2030." *World Health Organization* (2022). Print.

Amin, F., et al. "Degradation and Stabilization of Resin-Dentine Interfaces in Polymeric Dental Adhesives: An Updated Review." *Coatings* 12.8 (2022). Print.

Balhaddad, A. A. "Toward Dental Caries: Exploring Nanoparticle-Based Platforms and Calcium Phosphate Compounds for Dental Restorative Materials (Vol 4c, Pg 43, 2020)." *Bioactive Materials* 6.6 (2021): 1789-89. Print.

Bermudez, M., et al. "Bioactive Synthetic Peptides for Oral Tissues Regeneration." *Frontiers in Materials* 8 (2021). Print.

Bertassoni, L. E., and M. V. Swain. "Removal of Dentin Non-Collagenous Structures Results in the Unraveling of Microfibril Bundles in Collagen Type I." *Connective Tissue Research* 58.5 (2017): 414-23. Print.

Betancourt, D. E., P. A. Baldion, and J. E. Castellanos. "Resin-Dentin Bonding Interface: Mechanisms of Degradation and Strategies for Stabilization of the Hybrid Layer." *International Journal of Biomaterials* 2019 (2019). Print.

Blalock, J. E., and E. M. Smith. "Hydropathic Anti-Complementarity of Amino-Acids Based on the Genetic-Code." *Biochemical and Biophysical Research Communications* 121.1 (1984): 203-07. Print.

Brentani, R. R. "Biological Implications of Complementary Hydropathy of Amino-Acids." *Journal of Theoretical Biology* 135.4 (1988): 495-99. Print.

---. "Complementary Hydropathy and the Evolution of Interacting Polypeptides." *Journal of Molecular Evolution* 31.3 (1990): 239-43. Print.

Buzalaf, M. A. R., et al. "Ph-Cycling Models for in Vitro Evaluation of the Efficacy of Fluoridated Dentifrices for Caries Control: Strengths and Limitations." *Journal of Applied Oral Science* 18.4 (2010): 316-34. Print.

de Brito, O. F. F., I. L. M. de Oliveira, and G. Q. M. Monteiro. "Hydrolytic and Biological Degradation of Bulk-Fill and Self-Adhering Resin Composites." *Operative Dentistry* 44.5 (2019): E223-E33. Print.

de Sousa, J. P., et al. "The Self-Assembling Peptide P11-4 Prevents Collagen Proteolysis in Dentin." *J Dent Res* 98.3 (2019): 347-54. Print.

Derjaguin, B. V., V. M. Muller, and Y. P. Toporov. "Effect of Contact Deformations on the Adhesion of Particles." *Progress in Surface Science* 45.1-4 (1994): 131-43. Print.

Desouza, S. J., and R. Brentani. "Collagen Binding-Site in Collagenase Can Be Determined Using the Concept of Sense-Antisense Peptide Interactions." *Journal of Biological Chemistry* 267.19 (1992): 13763-67. Print.

Dorozhkin, S. V., and M. Epple. "Biological and Medical Significance of Calcium Phosphates." *Angewandte Chemie-International Edition* 41.17 (2002): 3130-46. Print.

Ezazi, M., et al. "Autonomous-Strengthening Adhesive Provides Hydrolysis-Resistance and Enhanced Mechanical Properties in Wet Conditions." *Molecules* 27.17 (2022). Print.

Fischer, N. G., et al. "Harnessing Biomolecules for Bioinspired Dental Biomaterials." *Journal of Materials Chemistry B* 8.38 (2020): 8713-47. Print.

Frassetto, A., et al. "Mechanisms of Degradation of the Hybrid Layer in Adhesive Dentistry and Therapeutic Agents to Improve Bond Durability-a Literature Review." *Dental Materials* 32.2 (2016): E41-E53. Print.

Goldberg, M., et al. "Dentin: Structure, Composition and Mineralization." *Front Biosci (Elite Ed)* 3.2 (2011): 711-35. Print.

Gungormus, M., et al. "Regulation of in Vitro Calcium Phosphate Mineralization by Combinatorially Selected Hydroxyapatite-Binding Peptides." *Biomacromolecules* 9.3 (2008): 966-73. Print.

Gungormus, M., et al. "Accelerated Calcium Phosphate Mineralization by Peptides with Adjacent Oppositely Charged Residues." *Acs Biomaterials Science & Engineering* 6.7 (2020): 3791-98. Print.

Gungormus, M., and F. Tulumbaci. "Peptide-Assisted Pre-Bonding Remineralization of Dentin to Improve Bonding." *Journal of the Mechanical Behavior of Biomedical Materials* 113 (2021). Print.

Habelitz, S., et al. "In Situ Atomic Force Microscopy of Partially Demineralized Human Dentin Collagen Fibrils." *Journal of Structural Biology* 138.3 (2002): 227-36. Print.

Hafner, A. E., et al. "Modeling Fibrillogenesis of Collagen-Mimetic Molecules." *Biophysical Journal* 119.9 (2020): 1791-99. Print.

Hardan, L., et al. "Effect of Collagen Crosslinkers on Dentin Bond Strength of Adhesive Systems: A Systematic Review and Meta-Analysis." *Cells* 11.15 (2022). Print.

Hegde, M. N., et al. "Salivary Alkaline Phosphatase and Calcium in Caries-Active Type Ii Diabetes Mellitus Patients: An in Vivo Study." *Contemp Clin Dent* 5.4 (2014): 440-4. Print.

Iijima, M., et al. "Effect of Solution Ph on the Calcium Phosphates Formation and Ionic Diffusion on and through the Collagenous Matrix." *Connective Tissue Research* 36.2 (1997): 73-83. Print.

Iliev, G., et al. "Shelf Life and Storage Conditions of Universal Adhesives: A Literature Review." *Polymers* 13.16 (2021). Print.

Jayaraj, D., and S. Ganesan. "Salivary Ph and Buffering Capacity as Risk Markers for Early Childhood Caries: A Clinical Study." *International Journal of Clinical Pediatric Dentistry* 8.3 (2015): 167-71. Print.

KONG, Jilie, and Shaoning YU. "Fourier Transform Infrared Spectroscopic Analysis of Protein Secondary Structures." *Acta Biochimica et Biophysica Sinica* 39.8 (2007): 549-59. Print.

Lamiable, A., et al. "Pep-Fold3: Faster Denovo Structure Prediction for Linear Peptides in Solution and in Complex." *Nucleic Acids Research* 44.W1 (2016): W449-W54. Print.

LeGeros, R. Z. "Calcium Phosphate-Based Osteoinductive Materials." *Chemical Reviews* 108.11 (2008): 4742-53. Print.

Li, Z., et al. "Promoting Effect of a Calcium-Responsive Self-Assembly Beta-Sheet Peptide on Collagen Intrafibrillar Mineralization." *Regen Biomater* 9 (2022): rbac059. Print.

Lin, Shan-Yang, Mei-Jane Li, and Wen-Ting Cheng. "Ft-Ir and Raman Vibrational Microspectroscopies Used for Spectral Biodiagnosis of Human Tissues." *Spectroscopy* 21.1 (2007): 1-30. Print.

Marshall, G. W., Jr. "Dentin: Microstructure and Characterization." *Quintessence Int* 24.9 (1993): 606-17. Print.

Meng, Elaine C, et al. "Tools for Integrated Sequence-Structure Analysis with Ucsf Chimera." *BMC bioinformatics* 7.1 (2006): 1-10. Print.

Meyer, F., et al. "Overview of Calcium Phosphates Used in Biomimetic Oral Care." *Open Dentistry Journal* 12 (2018): 406-23. Print.

Moradian-Oldak, J., and A. George. "Biomineralization of Enamel and Dentin Mediated by Matrix Proteins." *Journal of Dental Research* 100.10 (2021): 1020-29. Print.

Mukherjee, K., et al. "Enhancing Collagen Mineralization with Amelogenin Peptide: Toward the Restoration of Dentin." *Acs Biomaterials Science & Engineering* 6.4 (2020): 2251-62. Print.

Muliyar, S., et al. "Microleakage in Endodontics." *J Int Oral Health* 6.6 (2014): 99-104. Print.

Munchow, E. A., and M. C. Bottino. "Recent Advances in Adhesive Bonding - the Role of Biomolecules, Nanocompounds, and Bonding Strategies in Enhancing Resin Bonding to Dental Substrates." *Curr Oral Health Rep* 4.3 (2017): 215-27. Print.

Niu, L. N., et al. "Biomimetic Remineralization of Dentin." *Dental Materials* 30.1 (2014): 77-96. Print.

Oestervemb, N. "Bonding to Enamel and Dentin." *Textbook of Operative Dentistry*. 2 ed: JP Medical Publishers, 2012. Print.

Oladepo, S. A., et al. "Uv Resonance Raman Investigations of Peptide and Protein Structure and Dynamics." *Chemical Reviews* 112.5 (2012): 2604-28. Print.

Reis, A., et al. "Overview of Clinical Alternatives to Minimize the Degradation of the Resin-Dentin Bonds." *Oper Dent* 38.4 (2013): E1-E25. Print.

Sarikaya, R., et al. "Bioinspired Multifunctional Adhesive System for Next Generation Bio-Additively Designed Dental Restorations." *Journal of the Mechanical Behavior of Biomedical Materials* 113 (2021). Print.

Sarikaya, R., et al. "Probing the Mineralized Tissue-Adhesive Interface for Tensile Nature and Bond Strength." *Journal of the Mechanical Behavior of Biomedical Materials* 120 (2021). Print.

Sattabanasuk, V., et al. "Bonding of Resin Luting Cements to Dentine after Casein Phosphopeptide-Amorphous Calcium Phosphate (Cpp-Acp) Treatment." *International Journal of Adhesion and Adhesives* 54 (2014): 93-99. Print.

Scharnow, A. M., A. E. Solinski, and W. M. Wuest. "Targeting S. Mutans Biofilms: A Perspective on Preventing Dental Caries." *Medchemcomm* 10.7 (2019): 1057-67. Print.

Sheikh, Z., et al. "Mechanisms of in Vivo Degradation and Resorption of Calcium Phosphate Based Biomaterials." *Materials* 8.11 (2015): 7913-25. Print.

Song, L. Y., et al. "Multifunctional Monomer Acts as Co-Initiator and Crosslinker to Provide Autonomous Strengthening with Enhanced Hydrolytic Stability in Dental Adhesives." *Dental Materials* 36.2 (2020): 284-95. Print.

Spencer, P., et al. "Chemometrics-Assisted Raman Spectroscopy Characterization of Tunable Polymer-Peptide Hybrids for Dental Tissue Repair." *Frontiers in Materials* 8 (2021). Print.

Spencer, P., et al. "Threats to Adhesive/Dentin Interfacial Integrity and Next Generation Bio-Enabled Multifunctional Adhesives." *Journal of Biomedical Materials Research Part B-Applied Biomaterials* 107.8 (2019): 2673-83. Print.

Sreerama, N., and R. W. Woody. "Estimation of Protein Secondary Structure from Circular Dichroism Spectra: Comparison of Contin, Selcon, and Cdsstr Methods with an Expanded Reference Set." *Analytical Biochemistry* 287.2 (2000): 252-60. Print.

Steinbauer, P., et al. "Single-Molecule Force Spectroscopy Reveals Adhesion-by-Demand in Statherin at the Protein-Hydroxyapatite Interface." *Langmuir* 36.44 (2020): 13292-300. Print.

Tian, Z. L., et al. "Biomimetic Mineralized Hydrophilic Polyurethane Primers for Inducing Dentin Tubule Fillings." *Polymers* 14.21 (2022). Print.

Tsujimoto, A., et al. "Fatigue Bond Strength of Dental Adhesive Systems: Historical Background of Test Methodology, Clinical Considerations and Future Perspectives." *Japanese Dental Science Review* 58 (2022): 193-207. Print.

Vahedi, M., et al. "Comparison of Salivary Ion Activity Product for Hydroxyapatite (Ipha), Alkaline Phosphatase and Buffering Capacity of Adults According to Age and Caries Severity." *Journal of Dentistry* 13.4 (2012): 139-45. Print.

Wang, D., et al. "Preparation and Characterization of Crystalline Hydroxyapatite Induced by Self-Assembled Peptide and the Potential Application in Remineralizing Dentin." *Advanced Engineering Materials* 23.6 (2021). Print.

Wen, P. Y. F., et al. "Global Burden and Inequality of Dental Caries, 1990 to 2019." *Journal of Dental Research* 101.4 (2022): 392-99. Print.

Woolfolk, S. K., et al. "Peptide-Enabled Nanocomposites Offer Biomimetic Reconstruction of Silver Diamine Fluoride-Treated Dental Tissues." *Polymers* 14.7 (2022). Print.

Xia, K., et al. "Rgd- and Vegf-Mimetic Peptide Epitope-Functionalized Self-Assembling Peptide Hydrogels Promote Dentin-Pulp Complex Regeneration." *International Journal of Nanomedicine* 15 (2020): 6631-47. Print.

Ye, Q., et al. "Engineered Peptide Repairs Defective Adhesive-Dentin Interface." *Macromolecular Materials and Engineering* 302.5 (2017). Print.

Yuca, E., et al. "Reconfigurable Dual Peptide Tethered Polymer System Offers a Synergistic Solution for Next Generation Dental Adhesives." *International Journal of Molecular Sciences* 22.12 (2021). Print.

Zhang, J. H., et al. "Hydrolysis-Resistant and Stress-Buffering Bifunctional Polyurethane Adhesive for Durable Dental Composite Restoration." *Royal Society Open Science* 7.7 (2020). Print.

Zhou, Z., et al. "Remineralization of Dentin Slices Using Casein Phosphopeptide-Amorphous Calcium Phosphate Combined with Sodium Tripolyphosphate." *Biomedical Engineering Online* 19.1 (2020). Print.